

The Physical Characteristics of a CO₂ Seeping Fault: the implications of fracture permeability for carbon capture and storage integrity

Clare E. Bond^{1*}

Yannick Kremer²

Gareth Johnson³

Nigel Hicks⁴

Robert Lister⁵

Dave G. Jones⁵

Stuart Haszeldine³

Ian Saunders⁶

Stuart Gilfillan³

Zoe K. Shipton²

Jonathan Pearce⁵

¹Department of Geology and Petroleum Geology, University of Aberdeen, Meston Building, Kings College, Aberdeen, AB24 3UE, UK (clare.bond@abdn.ac.uk)

²Department of Civil and Environmental Engineering, University of Strathclyde, James Weir Building, Glasgow, G1 1XJ (yannick.kremer@strath.ac.uk; zoe.shipton@strath.ac.uk)

³School of Geosciences, University of Edinburgh, Grant Institute, Kings Buildings, James Hutton Road, Edinburgh, EH9 3FE (g.johnson@ed.ac.uk; stuart.gilfillan@ed.ac.uk; stuart.haszeldine@ed.ac.uk)

⁴Council for Geoscience, 139 Jabu Ndlovu Street, Pietermaritzburg, KwaZulu-Natal, South Africa 3200 (nhicks@geoscience.org.za)

⁵British Geological Survey, Environmental Science Centre, Nicker Hill, Keyworth, Nottingham NG12 5GG (trl@bgs.ac.uk; dgj@bgs.ac.uk; jmpe@bgs.ac.uk)

⁶Council for Geoscience, 280 Pretoria St, Silverton, Pretoria, 0184 (ians@geoscience.org.za)

*Corresponding Author clare.bond@abdn.ac.uk

Highlights

- CO₂ migration is spatially associated with the Bongwana fault fracture corridor.
- Cap rock permeability suggests that without fractures it would act as a flow barrier.
- Elevated CO₂ concentration and flux are measured across the fracture corridor.
- Fracture intensity and orientation variability creates permeability heterogeneity.
- Seismically unresolvable fracture networks may impact CO₂ storage capability.

Abstract

To ensure the effective long-term storage of CO₂ in potential geological storage sites, evaluation of leakage pathways to the surface should be undertaken. Here we use a series of natural CO₂ seeps along a fault in South Africa to assess the controls on CO₂ leakage to the surface. Geological mapping and detailed photogrammetry reveals extensive fracturing along the mapped fault trace. Measurements of gas flux and CO₂ concentration, across the fracture corridor, give maximum soil gas measurements of 27% CO₂ concentration, and a flux of 191 g m⁻² d⁻¹. These measurements along with observations of gas bubbles in streams and travertine cones attest to CO₂ migration to the surface. Permeability measurements on the host rock units show that the tillite should act as an impermeable seal to upward CO₂ migration. The combined permeability and fracture mapping data indicate that fracture permeability creates the likely pathway for CO₂ migration through the low permeability tillite to the surface. Heterogeneity in fracture connectivity and intensity at a range of scales will create local higher permeability pathways along the fracture corridor, although these may seal with time due to fluid-rock interaction. The results have implications for the assessment and choice of geological CO₂ storage sites, particularly in the assessment of sub-seismic fracture networks.

Keywords

Fracture permeability, CO₂ storage, leakage, natural analogue

1. Introduction

Climate change is generally recognized as a global 21st century challenge (Bernstein et al., IPCC, 2007). Anthropogenic greenhouse gas emissions, primarily CO₂, are extremely likely to have been the dominant driver of such change. CO₂ from fossil fuel combustion and industrial processes contributed 78% of the increase in GHG emissions between 1970 and 2010 (Field et al., IPCC, 2014). Carbon capture and storage (CCS) has been proposed to mitigate CO₂ emissions (Metz et al., IPCC, 2005). CCS is recognized as a bridging technology in energy production (e.g. Praetorius, and Schumacher, 2009), to mitigate the impact of CO₂ emissions, while renewable energy sources are developed. In order to expedite the deployment of CCS research is being undertaken to understand the reactivity and flow pathways of CO₂ in the subsurface (e.g Xu et al., 2003; Audigane et al., 2007) and to develop methods to measure, model and verify (MMV) geological CO₂ storage (Newell et al., 2008; Ringrose et al., 2013). Understanding the role of faults and fractures as fast fluid pathways, through overburden strata, to the surface is critical to ensure storage verification for engineered CCS sites.

Fracture controlled flow of CO₂ has been implicated in compromising the integrity of pilot CCS sites. For example, injection of CO₂ was halted at the In Salah CO₂ CCS pilot site due to the role of fractures in creating a conductive network through which CO₂ could migrate (e.g. Bond et al., 2013; Rinaldi and Rutqvist, 2013). To better understand the role of faults and associated fracture damage on controlling CO₂ flow pathways and flux rates, natural CO₂ seeps have been studied (e.g. Roberts et al., 2015). Examples of natural CO₂ seeps along faults include: the Paradox Basin Utah (e.g. Shipton et al., 2006); and the Apennines of Italy (e.g. Miller et al., 2004; Roberts et al., 2015). Here we describe the structural characteristics of the CO₂ seeping Bongwana Fault in KwaZulu-Natal, South Africa; to better constrain fracture and fault controlled CO₂ flow to the surface.

The Bongwana Fault is one of only two known examples of naturally seeping CO₂ in South Africa. The fault was identified during geological mapping between 1911-1916 by du Toit (1920), with CO₂ de-gassing along the fault first described by Young (1924). We present the first modern structural study of the physical characteristics of the fault, in terms of field exposure or a physical analysis of rock properties. We present new structural data from key locations where active CO₂ seeps occur along the fault as identified by Gevers (1941) and du Toit (1920). A hypothetical model of fracture-controlled permeability is proposed and refined by the field data. The results are discussed in the context of site selection and characterization at CCS sites where faults and fractures might play a role in permitting escape of CO₂ from a reservoir.

2. Geological Setting

The Ntlakwe-Bongwan Fault was identified during the mapping of Pondoland (Eastern Cape Province) and parts of the Alfred and Lower Umzimkulu Counties (KwaZulu-Natal) by du Toit (1920). The fault truncates sedimentary and igneous units of the Karoo Supergroup, as well as units of the Msikaba Formation in the south (Johnson et al., 2006). Within the study area, tillites and minor shales of the Dwyka Group, Karoo Supergroup, form the dominant surface lithologies. The tillite in southern KwaZulu-Natal has a thickness of ~450m (Thomas et al., 1990) and unconformably overlies coarse-grained sandstones and conglomerates of

the Msikaba Formation. The Msikaba Formation represents the assumed CO₂ reservoir, occurring as a 450m thick package in the Port Shepstone area which thickens southwards to 900m north of Port St Johns (Kingsley and Marshall, 2009).

The fault crops out on the surface over a trace length of 80 km (De Decker, 1981) with its northern extension known as the Bongwan, or Bongwana Fault (De Decker, 1981; Harris et al., 1997). The fault is related to Gondwana break-up which began at 180 Ma and continues today (Watkeys and Sokoutis, 1998). The zone of faulting in southern KwaZulu-Natal is about 70 km wide and defined by arcuate fault traces that change southwards from ENE-WSW to a north-south strike (Watkeys and Sokoutis, 1998). These fault systems correlate with the early stage, arcuate, Type I fault systems defined by Von Veh and Andersen (1990) in northern KwaZulu-Natal. Passive continental margin conditions have predominated since the late Jurassic (Maud, 1961; Dingle and Scrutton, 1974) with offshore faulting evident until the Cenomanian (Singh and McLachlan, 2003). The southeastern portion of southern Africa was subject to intense periods of epiorogenic uplift resulting in a marked onshore hiatus from the late Eocene to middle Miocene times (King, 1972; Frankel, 1972; Dingle and Scrutton, 1974; Grab and Knight, 2015), as well as in the Pliocene, where ~900m of uplift is postulated by Partridge and Maud (2000). To-date no faulting related to these uplift episodes has been recorded onshore, likely due to the erosional conditions that have prevailed since the early Cretaceous. Present day seismic activity is minimal, although a survey of micro-tremors using a single-station location method undertaken as a separate part of this study indicates a possible micro-earthquake of M~0.5 in 2007, the epicentre of which locates on the northern section of the Bongwana Fault near the abandoned gas works on Lot 7 (Site A – this study; see Figure 1).

Due to the homogeneous nature and thickness of the Dwyka Group tillites, fault displacement within the study area is hard to quantify. There are no mappable stratigraphic offsets in the study area (Figure 1). However, to the south along the Londobezi River a large graben is developed between two splays of the fault in which Ecca Group and Karoo Dolerite Suite rocks are preserved. Gevers (1941) suggests vertical offset in this region of 579m (1900 feet) with all units within the graben truncated by the fault system. These truncations allow for a maximum age definition for the faulting of ~179 Ma, based upon ⁴⁰Ar/³⁹Ar dating by Duncan et al., (1997) for the Karoo Dolerite Suite.

Watkeys and Sokoutis (1998) indicate that, due to intense subtropical weathering, the faulting pattern in southern KwaZulu-Natal is difficult to interpret. In areas of brecciation and silicification, the faults have a positive relief, a considerable aid to the delineation of the fault systems (Thomas, 1988). Gevers (1941) also describes the fault in many locations as a silicified feature that stands “proud of the ground”, with a range in the fault (fracture zone) width of between 0.3 m – 10 m wide. Gevers (1941) describes the fracture zones as being lenticular in shape and cropping out intermittently. The fault zone is chemically altered and marked by degradation of the tillite to a white, apparently pulverized, rock. The whitening of the rock is from the extensive kaolinisation and leaching of the tillite by CO₂ rich water (Gevers, 1941). According to Gevers (1941), within the Bongwana region, du Toit (1920) mapped splay and minor faults on either side, and parallel or sub-parallel, to the main fault, with splays extending for up to 1.6 km in length.

Young (1924) provided the first description of CO₂ degassing from Bongwana fault fissures. In his recordings of the exposure on Farm Lot 7 (Site A – this study), Young (1924) described CO₂ gas steadily bubbling to the surface in the Umzimkulwana River close to its west bank. It was at this site that a CO₂ bottling plant was established around 1924 to capture the CO₂ exhalations for commercial use (Gevers, 1941). On the neighboring farm (Lot 10), Young (1924) identified a two feet wide vertical zone of brecciated Dwyka Group tillite from which CO₂ de-gassed. Significantly higher CO₂ flux was noted by Young (1924) along the contact of brecciated Dwyka Group tillite with non-brecciated tillite described as being altered to soft clay. Analyses of the two gas samples, collected by Young (1924), gave CO₂ compositions of 98.3 % and 97.6 %. Gevers (1941) provides the most extensive description of the field sites seeping CO₂, including analysis of the gas. Further studies of the gas chemistry, including stable isotope analyses have been completed by Harris et al. (1997), reporting the CO₂ to have a $\delta^{13}\text{C}$ of -0.6 ‰ - +0.9 ‰ (PDB) and $\delta^{18}\text{O}$ 35.3-45.1 ‰ (SMOW). Gevers (1941) and Harris et al. (1997) suggest the CO₂ is sourced from the reaction of acidic ground water with carbonate rocks at depth. This hypothesis is plausible, as carbonate rocks of the Marble Delta Formation are seen cropping out ~30 km east of Bongwana (Figure 1), along structural basement strike, as a folded protolith enclave within Meso-proterozoic basement lithologies (Otto, 1973). Conversely with Hartnady (1985) who suggests generation of CO₂ by a mantle plume, with early carbonatite magma generation. Whatever the source, CO₂ has been seeping from the fault for some time because a series of travertine cones with CO₂ springs, some now dormant (Gevers, 1941; and observed in this study) attest to significant volumes of CO₂ over, at least, hundreds of years. Two of the localities identified by Gevers (1941) were visited, as well as a third mapped as a CO₂ exhalation by du Toit (1920). These locations are shown in Figure 1.

3. Models for CO₂ flow to the surface

Significant work has been undertaken within the oil and gas sector to determine the controls on the sealing capacity of faults (Yielding et al., 1997; Manzocchi et al., 1999; Bretan et al., 2003) and overburden caprocks (Grunau, 1987; Watts, 1987) to hydrocarbon fluids. This work is being used to inform predictions of the storage capacity and viability of potential CCS sites (Li et al., 2005; Li et al., 2006; Shukla et al., 2010), although it is recognized that faults and fractures may respond differently to CO₂, especially when pressurized CO₂ is injected (Rutquist, 2012; Verdon et al., 2015). Faults are known to act as both barriers and conduits to fluid flow (Sibson, 1995; Caine et al., 1996; Bense and Person, 2006), with the permeability characteristics of the fault plane and associated damage zone combining to determine a fault's overall permeability (Caine et al., 1996; Foxford et al. 1998; Aydin and Eyal, 2002). The geometry and heterogeneity of the whole fault zone, down to the micro-scale, determine a fault's permeability. Work on understanding and predicting fault (and off-fault) damage and its implications for permeability have mainly focused on normal faults within siliciclastic reservoir sequences (Caine et al., 1996; Hesthammer et al., 2000; Shipton and Cowie, 2003; Fossen et al., 2007; Farrell et al., 2014). Understanding of fault zone characteristics in other lithologies is less well developed, especially in relation to capacity for fluid flow. Studies on fault damage and implications for permeability in other lithologies include carbonates Agosta and Kirschner, (2003), Haines et al. (2016); basalts (Walker et al., 2013); and granitic gneiss (Lawther et al., 2016). A fault zone's potential to

act as a conduit for fluid is dependent on a number of factors that are not easily predicted (Fossen et al., 2007; Faulkner et al., 2010; Farrell et al., 2014).

A series of hypothetical models (Figure 2) show a range of potential fault zone permeabilities that may allow CO₂ flow to the surface at Bongwana. The models are based on understanding of different fault-rock permeabilities, originally proposed by Caine et al. (1996); and developed by others. Faulkner et al. (2010) give a summary. Here we consider these models by collection of field data and observations along the Bongwana Fault, combined with laboratory analysis to propose a site-specific model of CO₂ flow to the surface for Bongwana for future testing.

4. Methodology

A range of methodologies were employed to capture the structural characteristics of the Bongwana fault zone in an attempt to determine the potential role of the fault and associated fractures as pathways for CO₂ to the surface. Initial regional scale analysis was completed prior to field data collection using GoogleEarth™ and Aster imagery in combination with published geological maps (Gever, 1941; Thomas, 1988). In the field, these data were combined with GPS locations and structural measurements. High-resolution digital photography of fault zone outcrops were utilized for photogrammetry to create 3D virtual outcrop models. Desk-top digital analysis of the virtual outcrop models augment the in-field structural measurements. Outcrop scale maps of fault architecture were completed along with structural measurements and further detailed photography. Structural characterisation is augmented by gas (CO₂) flux and concentration measurements made at a single site and porosity and permeability measurements of the assumed reservoir (Msikaba Formation sandstones) and seal (Dwyka Group tillites) rocks. Each method employed is described in turn.

4.1 Structural Data

The app Fieldmove was used on an iPad Air 2 for collection of all structural data. Pre-loaded geo-tiffs of existing field maps and OpenStreet Map (mapbox.com) imagery were used in the field to aid in field site identification. In-field tracking was enhanced by Bluetooth connection of the iPad to a Garmin GLO for GPS and GLONASS location sensing. In-app functionality allows the user to define locations, take notes as in a field notebook, and take photos through access to the iPad's digital camera. Further, the app utilises the magnetometer, gyroscope and accelerometer within the iPad's hardware for use as a compass clinometer. Measurements of fracture orientation and dip were made and recorded directly on the iPad.

4.2 Virtual Outcrop Models

A Nikon D3200 SLR was used with a fixed lens (35mm) to collect digital photographs of outcrops for photogrammetry. The method requires multiple photographs to be taken orthogonal to the outcrop surface, with an approximate 60 % over-lap. The photographs are georeferenced and a scale and orientation is used in each photo-set to allow for later scaling and geo-referencing of the virtual outcrop models. Each evening the photographs were downloaded and processed in Photoscan-pro software to create a 3D virtual outcrop model. The technique and its use in geology is described by various authors (e.g. Roncella et al., 2005; Bemis et al., 2014; Johnson et al., 2014; Salvini et al., 2015). Creating virtual outcrop

models during the fieldwork allows for checks to be made of the photogrammetric model to see if the photographs have the required overlap and coverage, so that further photos may be acquired if needed to create a full virtual outcrop model.

Oriented ortho-rectified photographs (orthophotos) were created from the virtual outcrop models; these were imported into Move software, scaled and geo-referenced, where digital interpretation of the fracture sets was undertaken. The pixel size of the imagery was kept constant at 300 dpi. The software is used to determine fracture attributes, such as orientation and length; as well as to determine if multiple fracture sets are present. The digitised fracture datasets were input into a MATLAB script to determine fracture intensity for each virtual outcrop using the circular scan-line method of Mauldon et al. (2001).

4.3 Gas Flux and Composition Sampling

Soil gas measurements were made using probes consisting of an 8 mm diameter (4 mm internal diameter) stainless-steel tube onto which two solid steel cylinders were welded to act as pounding surfaces when installing and removing the probes with a co-axial hammer. Prior to insertion, a sacrificial tip was fitted to the bottom of the probe to prevent blockage. The probes were inserted to a depth of 85-90 cm. In situ soil gas measurements of CO₂, H₂S, CH₄, and O₂ concentrations were made using a Geotechnical Instruments GA2000 portable gas analyser. CO₂ flux measurements were taken using a West Systems portable flux meter with a LICOR LI-820 IR detector connected via Bluetooth to a Trimble Juno palm-top computer (PDA) with built-in GPS. Measurements took 1–3 min depending on the soil flux rate. Flux was measured before soil gas to minimise disturbance of the flux. The instruments were calibrated before and after the fieldwork using certified calibration gases.

4.4 Porosity and Permeability Analysis

Porosity and permeability analyses were made on samples of Msikaba Formation sandstone (3 orthogonal cores) and Dwyka Group tillite, from outside the obvious fault/fractured area (2 cores – at right angles). Porosity measurements were made on core samples using helium (He) gas, on an Edinburgh Petroleum Ltd, Mk. 2 Helium gas porosimeter. Permeability measurements were made on the core samples using a Jones permeater with nitrogen (N₂) gas. A Hassler sleeve was used to pressurize the sample to 400 psi (2.76 MPa), and five repeat measurements at different fluid pressures on the high pressure gauge were measured. The results were corrected using a Klinkenburgh correction and the mean value used.

5. Results and Analysis

Within the study area the fault is expressed in a series of outcrops that are relatively sparse with respect to the fault length and which vary in character from highly fractured zones to apparently 'pulverised' rock. Nowhere is the full width of the fault obviously exposed. Small sections of fractured Dwyka Group tillite are observed. The fault zone surface expression is defined by distributed fractured rock outcrop, defining a fracture corridor, rather than a discrete single fault surface, or fault slip plane and damage zone. Three localities of CO₂ degassing along the fault trace informed the study (Figure 1).

Site A, occurs on Farm Lot 7 alongside the Umzimkulwana River east of Bongwana rail siding. Here CO₂ is observed effervescing in the Umzimkulwana River where the road bridge crosses the river; on the western bank of the river pools of water in river bank sand also show CO₂ bubbles. The outcrop at Site A is approximately 2.5 m x 1.5 m, sited next to the river and consists of fractured Dwyka Group tillite. The exhalations at this site have a high flux rate with Gevers (1941) indicating that exhalations identified on the neighbouring farm, Lot 10, measured 30 ft³ minute⁻¹ (0.014 m³s⁻¹) from a 5 inch (0.127 m) diameter pipe in 1924.

Site B (Figure 1), occurs 9 km south of Site A on the Manzimhlanga River, near Mjaja; here several outcrops of faulted and fractured Dwyka Group tillite crop out. CO₂ de-gassing is observed as bubbles in the nearby river, but the volume is minimal in comparison to Site A. Three distinct outcrops are described at Site B, which are characterized both by leaching and whitening of the rock, but with areas of iron staining and some silicification.

Site C (Figure 1) is the southernmost of the known CO₂ emissions along the Bongwana Fault occurring on the northern and southern banks of the Umtamvuna River where well developed travertine cones and CO₂ springs are identified. Four travertine cones are developed atop large travertine mounds ~50-100m in diameter. Two cones occur on the northern bank and are by far the largest (~15m diameter). These cones are only partially active with minor CO₂ gas and water seeps identified. On the southern bank, two smaller cones are identified, both of which are active. Both issue CO₂ gas and water, with the larger "Cone Spring" represented by a steep-sided cone ~1 m in diameter and 80 cm high. The other spring occurs ~5 m east, as a flat cone termed the "Mound Spring". As well as basic mapping of the travertine cones, structural measurements were made at two key localities in the vicinity of the cones where fractured and brecciated outcrops were observed that have not previously been described.

5.1 Regional Trend and Structural Data

The outcrops visited are linearly aligned, approximately North-South over a horizontal distance of 15 km. The outcrops fall on the line of the Bongwana fault mapped by du Toit (1920) and published by Gevers (1941) (Figure 3).

Fracture orientations were measured at all three localities. Primary fractures identified in the field have N-S trends (Figure 3a – rose diagrams). Poles to fractures at Sites A, B and C have kappa distributions of 1.13, 2.58 and 2.5 respectively (where smaller kappa indicates a tighter clustering of fracture orientations). The fractures are sub-vertical with a mean dip between 82°-89° at the three sites. Fractures dip in both directions around a mean fracture strike for Site A of 169° and at Site C 006°. The fractures measured at Site B appear more dispersed in nature (Figure 3a) with a mean fracture strike orientation approximately NE-SW (a mean dip of 82° and a strike direction of 029°), but with significant dispersion within the NE and SW stereonet segments (Figure 3a).

At Sites B and C multiple sub-sites form the dataset (Figure 3c and d) between 20 and several 100 m apart. Stereonet plots from individual outcrop sub-sites show more consistency in fracture strike orientation, so the dispersion in fracture orientation is created

from the amalgamation of the fracture data collected at the multiple sub-sites. Outcrop site Bi shows a fracture distribution similar to Site A with a predominant primary fracture set trend of approximately N-S, with a NW-SE oriented secondary fracture set. Sites Bii, iii, iv all show fractures in a NE-SW direction. At site Bii a NE-SW fracture strike is most prevalent. The rock here appears grey-white in colour and has the consistency of white flour when hammered. Sites Bii and Biii c. 20 m apart, are linked by almost continuous outcrop, in which the along-strike change in fracture trend can be observed. The mean fracture dip at site Bii is 82°, with a mean strike of 055°; at site Biii the mean dip is 82° with a mean strike of 026°. At site Biii the fractures dip consistently to the east. The rock character also changes, as you move away from the apparently pulverized rock at Bii into the coherent rock at Biii where primary and secondary fracture sets can be identified. Often the secondary fractures form with horsetail geometries, splaying from primary fractures or filling the rock space between approximately N-S oriented primary fractures. These geometries are also identified in analysis of the virtual outcrop models and fault architecture mapping. The change in fracture orientation at site B corresponds to a bend in the fault line on the surface, according to the mapping of du Toit and Gevers (1941). This bend changes the fault orientation from approximately N-S 006° at Site C to an approximate NE-SW 029° at Site B, (Figure 3b).

At two sites slickensides could be measured on fracture/fault surfaces. At Site Cii a small fracture surface oriented with a strike of 013 and a dip of 82° had three measurable slickensides. The mean slickenside trend is 337 with a plunge of 77°. The slickensides are approximately dip-slip (vertical) (figure 3b). At Site Biv a larger fracture/fault surface is exposed with numerous slickensides, 14 slickenside lineation measurements were made on the surface. In figure 3b a mean fracture plane surface is plotted (great circle) with a strike of 031 and a mean dip of 82°, the slickensides are sub-parallel with a mean slickenside trend is 050 with a plunge of 72°. The slickensides at Site Biv are slightly oblique to dip-slip, by c. 20° to the NE.

5.2 Fault Architecture Mapping from Virtual Outcrop Models

Virtual outcrop models were made at all three sites. Virtual outcrop models of five fractured surfaces from the three sites have been digitally interpreted on orthorectified photographs. Fracture orientations derived from the models (Figure 4a-e, stereonet), are consistent with in-field measurements (Figure 3, stereonet), with a main fracture set trending c. N-S and secondary sets either trending c. E-W, or as a conjugate set bisecting an E-W trend. Mapped fractures at Site Bi and Biii (Figure 4b and 4c), show the horsetail geometries and fracture splays.

Using a custom MATLAB script, we use the circular scanline method of Mauldon et al. (2001) to create fracture density plots (number of fractures per m²) for each digitally interpreted outcrop (Figure 4a-e). This approach defines a circular sampling window, from which the number of fracture endpoints (m) within the circle and the number of fracture intersections (n) with the circle are recorded. From these two statistics, the fracture density, intensity and mean trace length can be calculated. The script uses a moving window approach to calculate the statistics for a large number of circles at different locations, resulting in a map of fracture intensity variation. The accuracy of this method depends on the number of endpoints in the circle, and therefore on the size of the circle compared to typical fracture

spacing. Rohrbaugh et al. (2002) suggest that the scan-circle radius should exceed typical block size. To accurately determine the minimum scan radius required for our fracture maps, we calculate these statistics for different circle radii at several locations. Figure 5 shows a plot of the three properties, density, intensity and mean trace length, against circle radius for site Ci. At this location, the statistics stabilise at a fracture radius of at least 8 cm.

The fracture density maps created can be used to visualise and examine the heterogeneity of the fracture network. Calculated values are artificially low near the edges of the map, as no fractures are mapped in poorly exposed areas. As such, representative values for the fracture density at this location must be taken at least one radius distance (8 cm) away from the edge of the rock outcrop. This results in typical fracture densities ranging from 1500 – 3000 fractures m^{-2} at Site Ci. For this site fracture intensity ranges from 40 to 120 fractures m^{-1} , and mean trace lengths range from 5 to 15 cm. At the nearby site Cii, 100 m away, the fracture density is a maximum of 11 fractures m^{-2} (Figure 4e). Fractures are mainly unfilled, e.g. Sites A and C. At these sites where red-brown staining around the fractures (thin halos up to 0.5 cm) and coatings on fracture surfaces is interpreted as evidence for past fluid-flow. At Site B fractures appear to be cemented, as part of the pervasive (in the vicinity to fractures) chemical alteration of the rock.

5.3 Gas Flux and composition measurements

Gas flux and composition measurements were made at Site C along a transect perpendicular to and crossing the trend of the main fault line. The locality chosen was on the Northern bank of the Umtamvuna River between mapped active gas exhalations (Figure 6). The results of the gas flux and composition measurements are shown in map view, with circles scaled for flux (Figure 6a) and graphically (Figure 6b). Falling on the predicted fault line (zero on the x-axis of the graph) the maximum percentage of CO_2 in the captured gas is 27 %, with a flux of $191 \text{ g m}^{-2} \text{ d}^{-1}$. Away from the predicted fault line (50-80 m) the flux and CO_2 composition recorded diminish to 1 % or below, and $17\text{-}26 \text{ g m}^{-2} \text{ d}^{-1}$. A symmetrical pattern is seen on either side of the fault with no observed difference in the footwall or hangingwall of the structure. The results support the assertion that the fault and associated deformation structures are controlling migration of CO_2 to the surface.

5.4 Porosity and Permeability data

Porosity and permeability measurements were made on three orthogonal cores of Msikaba Formation sandstone collected in the Oriibi gorge. The sandstone is quartz dominated and shows a coarsening-upward sequence within beds. The sample, of a bed approximately 20 cm thick, contains quartz pebbles (2-10 mm) at its base fining up to <1 mm. The cores were taken across bedding and in two orthogonal orientations parallel to bedding. Samples of apparently undeformed and unaltered Dwyka Group tillite from Site Bii, less than 1 m from highly altered tillite in the 'fault zone', were also cored in two orthogonal directions. The tillite has a fine-grained grey matrix with clasts in the samples up to 10 mm in diameter, but generally clasts are 2-3 mm in size. Samples of fractured and altered tillite disintegrated when cut or cored using water-cooled mechanisms, supporting the assertion of alteration to clays, so were not suitable for core analysis.

The results of the analyses are shown in Table 1. The unaltered Dwyka Group tillite has a high porosity (c. 20%), compared to the Msikaba Formation sandstone (c. 4-5%) but a lower effective permeability 1×10^{-2} . Figure 7 shows the samples plotted on a porosity-permeability plot alongside data from different types of sandstones from Lake (2007) - Society of Petroleum Engineers (SPE) (Petrowiki, accessed 2016). The Msikaba Formation sandstone falls within the range of consolidated sandstones (0.18 -0.27 mD), whilst the tillite has a permeability at the lower end of consolidated sandstone and the top end of tight sands (0.06 – 0.07 mD).

6. Discussion

The Bongwana Fault is unusual in its expression. Our observations of dip-slip slickensides on steeply dipping fracture surfaces support those of Gevers (1941) who described dip-slip slickensides on an almost vertical fault. However, no distinct fault surface is observed in the field. The fault displacement-length characteristics at the lower end of those predicted by global compilations (e.g. Walsh and Watterson, 1988; Schlische et al., 1996; Kim and Sanderson, 2005). For an 80 km long normal fault, displacement in the order of 80 m-8 km would be expected based on the range of published displacement length data, compared to the 579 m estimated throw observed by Gevers (1941). These observations suggest that the Bongwana Fault is a deep-seated basement fault, or series of amalgamated faults that may have had an earlier strike-slip history. Given the lack of observed piercing points, the amount of strike slip on the fault is not quantified.

Porosity and permeability measurements of selected rock samples attest to a potential CO₂ reservoir at depth and an effective cap rock seal. The Dwyka Group tillite (assumed cap-rock seal) has a high porosity but low effective permeability (1×10^{-2} mD). In contrast, the permeability of the assumed CO₂ reservoir, the Msikaba Formation sandstone, is 1×10^{-1} mD, within the range of known consolidated sandstones that form hydrocarbon reservoirs, whereas the tillite has a permeability at the high-end of tight sands (Figure 7). Tight sand reservoirs in a hydrocarbon setting are reliant on fracture permeability for effective hydrocarbon flow. The fractures identified in the field associated with the Bongwana Fault are therefore the likely conduit for CO₂ from the Msikaba Formation sandstone to the surface.

The dominant fracture set parallels the fault with fractures oriented c. N-S, although there is local variability in orientation. Further minor fracture sets are also seen, with significant local heterogeneity in orientation and intensity. Fractures are observed to swing in orientation towards the NE-SW at a mapped bend in the fault. Fracture connectivity and hence bulk permeability is predicted to be higher in the fault bend zone, where fracture sets with different orientations intersect. Fault bends often correspond to local high stress anomalies, and stress rotations resulting in a greater diversity in fracture orientation and an increase in fracture intensity, permeability and fluid flow (e.g. Curewitz and Karson, 1997; Kattenhorn et al., 2000; Tamagawa and Pollard, 2008). The current stress regime in the Bongwana Fault area, is extension oriented approximately NNW-SSE (Brandt, 2011). This suggests that the NE-SW oriented fault bend on the Bongwana Fault at Site B would be in net extension and some rotation of the local stress field would be expected.

In the detailed fracture intensity maps (Figure 4), shorter length 'small scale' fractures, oriented orthogonal or sub-orthogonal to the c. N-S fractures, are captured. These fractures are missing from in-field measurements at Sites A and C (Figure 3). We suggest this is the result of in-field sampling bias (e.g. Hunter and Donovan, 2005; Bond et al., 2007; Bond, 2015) in which the more dominant (longer length and 'thicker') N-S fractures have been preferentially sampled. Although, often 'hairline' in width the increase in fracture connectivity afforded by an orthogonal linking fracture set can drastically increase potential fracture permeability (e.g. Watkins et al., 2015). "Linking" fractures at Site B (the fault bend) show horsetail and splay geometries, and in some outcrops these fractures dominate the fracture population e.g. Site Bii (figure 3c).

High permeability fracture-dominated pathways controlling spatially distinct CO₂ leakage along a fault in Utah (Burnside et al., 2013). At the Utah site ancient travertine cones record a 400,000+ year history of CO₂ exhalation along the fault, concentrated along high permeability pathways controlled by areas of high fracture density (Dockrill and Shipton, 2010), and with a history of sealing and fluid pathway displacement along the fault (Burnside et al., 2013). At Bongwana, there is evidence of fluid-rock interaction, notably at the bend in the fault, where Dwyka Group tillite appears to be altered to kaolinite. So although this fault-bend area is predicted as having a high fracture permeability with respect to the range in fracture orientations, it is possible that this may be reduced or sealed completely due to mineral reactions during CO₂ flux.

Direct evidence for CO₂ surface exhalations are seen with the presence of travertine cones and gas bubbles effervescing in rivers that cross the mapped fault line. Measurements of ground gas flux and CO₂ concentration across the fracture corridor show a significant flux of CO₂ (191 g m⁻² d⁻¹), with 27% CO₂ measured in the soil gas. The % of CO₂ is significantly above normal back ground levels of <1%. Within c. 50 m of the predicted fault line (on both sides) the CO₂ concentrations and gas flux measurements are consistent with non-elevated levels. Although, we can spatially correlate the CO₂ flux to the fault-line diffusion of the CO₂ through the soil will likely obscure any spatial heterogeneity in the flux associated with fractures.

The CO₂ flux is lower than other cited examples of CO₂ fluxes along fault lines. Gouveia et al. (2005) and Gouveia and Friedmann (2006) measure modern exhalation of CO₂ flux from Crystal Geyser in Utah of 30 tonnes d⁻¹. The flux here however is up a well that was drilled into the fault, giving a point source of CO₂. Values by Roberts et al. (2015) give an average flux of between 10-100 tonnes d⁻¹ for seeps in Italy, although the area over which these values were recorded is not detailed. Annunziatellis et al. (2008) record flux values of CO₂ up faults in the Latera Caldera in Central Italy. The mean CO₂ flux value (1700 g m⁻² d⁻¹) here is very high due to the maximum value of 49563 gm⁻² d⁻¹, while the median value (331 gm⁻² d⁻¹). Data from Beaubien et al. (2008), also from the Latera Caldera, give maximum values of over 90% CO₂ in soil gas and a maximum flux greater than 1600 g m⁻² d⁻¹. Background values were less than 5% and the flux is generally below 10 g m⁻² d⁻¹. Measurements from a traverse near the Laacher See in Germany showed max CO₂ concentrations exceeding 80% and maximum fluxes over 500 g m⁻² d⁻¹. Away from CO₂ vents concentrations were below 5% CO₂ with a flux below 50 g m⁻² d⁻¹ (Krueger et al 2011): these data are most comparable to Bongwana. Data from a site near Florina, Greece give max CO₂ concentrations also over

80%, with the highest fluxes exceeding $2000 \text{ g m}^{-2} \text{ d}^{-1}$ (max over $9000 \text{ g m}^{-2} \text{ d}^{-1}$). Background values here are similar to those found at Laacher See and Bongwana (Zigou et al., 2013).

Our favored model for CO_2 flux to the surface at Bongwana is summarized schematically in Figure 8a. We propose that a blind fault is likely genetically linked to the surface through a connected fracture network, exposed on the surface as a fracture corridor, and through which CO_2 and other fluids migrate. In Figure 8b a simplified block diagram illustrates the proposed model for a discrete fault-slip surface and associated fractures at depth connected to the surface through a fracture network. This model differs from the proposed models in Figure 2, which rely on a continuous fault and associated damage zone cropping out at the surface. A theoretical graph of permeability is shown cutting the fracture network (Figure 8b). The permeability is determined by the open fracture network permeability. The jaggedness of the permeability graph represents the likely heterogeneities in fracture permeability resulting from the mapped variations in fracture intensity and connectivity mapped, and potential fracture seal due to fluid-rock interaction. Such heterogeneities captured in 2D in the graph would be mirrored along strike resulting in a 3D heterogeneity of CO_2 flux to the surface.

The true heterogeneity of the fracture network's permeability in controlling CO_2 flow to the surface is untested here. To better understand the genetic link between the fracture network and CO_2 surface exhalation, direct measurements of CO_2 flux on rock outcrops mapped for fractures is proposed as a focus for future work. This provides challenges in ensuring a seal between the rough outcrop surface and the gas capture chamber, but would provide direct evidence of the role of the fracture network permeability in controlling CO_2 flux. Given the observation of reaction to kaolinite in the Dwyka Group tillite, in a highly fractured zone, direct measurements of CO_2 flux on fractured outcrop should be combined with detailed petrography to assess the role of fracture seal from fluid-rock interaction. Together such a study could provide not only a present day picture of fracture permeability and CO_2 flux, but a history of flow and fracture seal.

The connectivity of the Bongwana Fault to the surface through a fracture network has risk implications for fault-bounded CCS sites. For CCS sites that are fault bounded at depth, fractures either associated with the initial faulting or that have formed subsequently due to fault evolution and reactivation may require re-evaluation. Work to better understand the evolution of damage resulting from fault growth and linkage (e.g. Peacock, 2002; Childs et al., 2009; Choi et al., 2016) may inform such evaluations. The observations at Bongwana suggest that rock damage associated with a propagating fault tip (e.g. McGrath and Davison, 1995) at depth may create fracture permeability ahead of a discrete slip surface; as seen in hydrothermal systems (Curewitz and Karson, 1997). The bend in the fault, at Site B, could be the result of linkage of two initial fault segments, with the extra fracture damage in this area the result of fracturing ahead of the propagating fault tip prior to linkage. The fracture geometries (horsetails and splays) and orientations are consistent with such a model (Choi et al., 2016). If Site B is a fault linkage zone then we would predict higher fracture permeability at linkage zones, as described by other authors (e.g. Curewitz and Karson, 1997; Rotevatn and Bastesen, 2014).

Fracture networks such as those at Bongwana will not be seismically resolvable, and fault linkage zones may be hard to distinguish in seismic imagery. Interpretation of seismic data of traps for CO₂ storage, may suggest an intact top seal, but could be jeopardized by an un-imaged connected fracture network. Clear understanding of fault geometries and evolution within a regional and local stress field (e.g. Kattenhorn et al., 2000; Healy, 2008) should help to predict fracture deformation patterns. Such studies are crucial to understanding how faults and associated deformation may affect storage integrity for potential fault bounded CCS sites. This understanding is particularly important for fracture networks that are below seismic image resolution.

7. Conclusions

Permeability measurements of Dwyka Group tillite suggest that CO₂ stored at depth should be sealed by the tillite. However, field observations of elevated fluid fluxes, and the presence of travertine cones on the surface purport CO₂ flux to the surface. The CO₂ exhalations are spatially correlated with a fracture corridor known as the Bongwana Fault. We propose that the CO₂ is exploiting the fracture network to exhale on the surface. Mapped heterogeneity in fracture orientation and intensity suggest that CO₂ flux to the surface will be controlled by localized zones of high permeability along the fracture corridor. Zones of high permeability are created by fracture network connectivity rather than a discrete fault zone. Fracture network connectivity is enhanced by local fault bends that result in fractures with a greater diversity in orientation, as well as local heterogeneity in fracture intensity and connectivity. Further, the spatial distribution of permeability within the fracture network is likely to vary through time as fluid rock interaction seals the fractures.

The Bongwana Fault, along with other global examples of natural CO₂ seeps, provides evidence that even when there is both a high permeability reservoir and low permeability caprock that localized fracture deformation can result in seal breach. Fractures are often below seismic image resolution, creating an unknown risk in the evaluation of CCS sites. Better understanding of deep-seated fault geometries and deformation around faults, particularly at faults tips and in fault linkage zones, in their regional and local stress field should aid in the prediction of areas of high fracture intensity and hence potential high-risk leakage zones in CCS sites.

Acknowledgements

The authors would like to acknowledge the financial support of the UK CCS Research Centre (www.ukccsrc.ac.uk) in carrying out this work. Author Kremer is supported by NERC grant NE/N015908/1. The UKCCSRC is funded by the EPSRC as part of the RCUK Energy Programme. Midland Valley Exploration are thanked for an academic license for Move. Porosity and permeability analysis were undertaken in the University of Aberdeen Petrophysics laboratory with the aid of Sophie Harland. The South African National Energy Development Institute (SANEDI) Stakeholder Engagement team under the South African Centre for Carbon Capture & Storage (SACCCS) is thanked for making the scientific work possible. The National, Provincial and Local Government structures including Traditional Authorities, Municipalities, landowners and local residents are thanked for granting permission to conduct the monitoring in the areas of interest. CGS staff are thanked for

their assistance and support in the field. We thank two anonymous reviewers for their comments, which helped to improve the manuscript.

References

Agosta, F., and Kirschner, D.L., 2003. Fluid conduits in carbonate-hosted seismogenic normal faults of central Italy. *J. Geophys. Res.* 108, B4. <http://dx.doi.org/10.1029/2002JB002013>.

Audigane, P., Gaus, I., Czernichowski-Lauriol, I., Pruess, K. and Xu, T., 2007. Two-dimensional reactive transport modeling of CO₂ injection in a saline aquifer at the Sleipner site, North Sea. *American Journal of Science*, 307(7), pp.974-1008.

Aydin, A. and Eyal, Y., 2002. Anatomy of a normal fault with shale smear: Implications for fault seal. *AAPG bulletin*, 86(8).

Beaubien, S.E., Ciotoli, G, Coombs, P, Dictor, M. C., Krüger, M, Lombardi, S, Pearce, J.M. and West, J.M. 2008. The impact of a naturally occurring CO₂ gas vent on the shallow ecosystem and soil chemistry of a Mediterranean pasture (Lattera, Italy). *International Journal of Greenhouse Gas Control*, Vol. 2, 373-387.

Bense, V.F. and Person, M.A., 2006. Faults as conduit-barrier systems to fluid flow in siliciclastic sedimentary aquifers. *Water Resources Research*, 42(5).

Bemis, S.P., Micklethwaite, S., Turner, D., James, M.R., Akciz, S., Thiele, S.T., and Bangash, H.A., Ground-based and UAV-based photogrammetry: A multi-scale, high-resolution mapping tool for structural geology and paleoseismology. 2014 *Journal of Structural Geology*, v. 69, p. 163–178, doi: 10.1016/j.jsg.2014.10.007

Bernstein, L., Bosch, P., Canziani, O., Chen, Z., Christ, R., Davidson, O., ... & Kundzewicz, Z. (2007). IPCC, 2007: climate change 2007: synthesis report. Contribution of working groups I, II and III to the Fourth Assessment Report of the Intergovernmental Panel on Climate Change. *Intergovernmental Panel on Climate Change, Geneva*. < <http://www.ipcc.ch/ipccreports/ar4-syr.htm>.

Bond, C. E., Z. K. Shipton, R. R. Jones, R. W. H. Butler, and A. D. Gibbs. 2007. Knowledge transfer in a digital world: Field data acquisition, uncertainty, visualization, and data management. *Geosphere* 3, no. 6 (2007): 568-576.

Bond, C. E. 2015. Uncertainty in structural interpretation: Lessons to be learnt. *Journal of Structural Geology*, 74, 185-200.

Bond, C.E., Wightman, R. & Ringrose, PS. (2013). 'The influence of fracture anisotropy on CO₂ flow'. *Geophysical Research Letters*, vol 40, no. 7, pp. 1284-1289.

Bretan, P., Yielding, G. and Jones, H., 2003. Using calibrated shale gouge ratio to estimate hydrocarbon column heights. *AAPG bulletin*, 87(3), pp.397-413.

Burnside, N.M., Shipton, Z.K., Dockrill, B. and Ellam, R.M., 2013. Man-made versus natural

667 CO₂ leakage: A 400 ky history of an analogue for engineered geological storage of CO₂.
668 *Geology*, 41(4), pp.471-474.

669 Brandt, M. 2011. Seismic Hazard in South Africa Council for Geoscience Report number:
670 2011-0061 © Copyright 2011. Council for Geoscience.

671 Caine, J.S., Evans, J.P. and Forster, C.B., 1996. Fault zone architecture and permeability
672 structure. *Geology*, 24(11), pp.1025-1028.

673
674 Childs, C., Manzocchi, T., Walsh, J.J., Bonson, C.G., Nicol, A. and Schöpfer, M.P., 2009. A
675 geometric model of fault zone and fault rock thickness variations. *Journal of Structural*
676 *Geology*, 31(2), pp.117-127.

677
678 Choi, J.H., Edwards, P., Ko, K. and Kim, Y.S., 2016. Definition and classification of fault
679 damage zones: A review and a new methodological approach. *Earth-Science Reviews*, 152,
680 pp.70-87.

681
682 Curewitz, D. and Karson, J.A., 1997. Structural settings of hydrothermal outflow: Fracture
683 permeability maintained by fault propagation and interaction. *Journal of Volcanology and*
684 *Geothermal Research*, 79(3), pp.149-168.

685
686 De Decker, R.H., 1981. Geology of the Kokstad area. Explan. Sheet 3028. Dep, Miner, Energy
687 Affairs. Pretoria.

688
689 Dingle, R.V. and Scrutton, R.A., 1974. Continental break-up and the development of Post-
690 Paleozoic sedimentary basins around southern Africa. *Bulletin, Geological Society of*
691 *America*, 85, 1467–1474.

692
693 Dockrill, B. and Shipton, Z.K., 2010. Structural controls on leakage from a natural CO₂
694 geologic storage site: Central Utah, USA. *Journal of Structural Geology*, 32(11), pp.1768-
695 1782.

696
697 Duncan, R.A., Hooper, P.R., Rehacek, J., Marsh, J. and Duncan, A.R., 1997. The timing and
698 duration of the Karoo igneous event, southern Gondwana.

699
700 du Toit, A.L., 1946. The geology of parts of Pondoland, East Griqualand. Explanation, Cape
701 Sheet 35, Geological Survey of South Africa.

702
703 Foxford, K.A., Walsh, J.J., Watterson, J., Garden, I.R., Guscott, S.C. and Burley, S.D., 1998.
704 Structure and content of the Moab fault zone, Utah, USA, and its implications for fault seal
705 prediction. *Geological Society, London, Special Publications*, 147(1), pp.87-103.

706
707 Farrell, N.J.C., Healy, D. & Taylor, C.W. (2014). 'Anisotropy of permeability in faulted porous
708 sandstones'. *Journal of Structural Geology*, vol 63, pp. 50-67.

709
710 Faulkner, D., Jackson, C., Lunn, R., Schlische, R. W., Shipton, Z., Wibberley, C., & Withjack, M.
711 O. 2010. A review of recent developments concerning the structure, mechanics and fluid

712 flow properties of fault zones. *Journal of Structural Geology*, 32(11), 1557-1575.
713 [10.1016/j.jsg.2010.06.009](https://doi.org/10.1016/j.jsg.2010.06.009)
714
715 Field, C.B., Barros, V.R., Dokken, D.J., Mach, K.J., Mastrandrea, M.D., Bilir, T.E., Chatterjee,
716 M., Ebi, K.L., Estrada, Y.O., Genova, R.C. and Girma, B., 2014. IPCC, 2014: Climate Change
717 2014: Impacts, Adaptation, and Vulnerability. Part A: Global and Sectoral Aspects.
718 Contribution of Working Group II to the Fifth Assessment Report of the Intergovernmental
719 Panel on Climate Change.
720
721 Fossen, H., Schultz, R.A., Shipton, Z.K. and Mair, K., 2007. Deformation bands in sandstone: a
722 review. *Journal of the Geological Society*, 164(4), pp.755-769.
723
724 Frankel, J.J., 1972. Distribution of Tertiary sediments in Zululand and southern Mozambique,
725 southeast Africa. *American Association of Petroleum Geologists, Bulletin*, 56, 2415-2425.
726
727 Gevers, T.W., 1941. Carbon Dioxide Springs and Exhalations in Northern Pondoland and
728 Alfred County Natal. *Transactions of the Geological Society of South Africa*. 44, 233-301
729
730 Gouveia, F.J., and Friedmann, S.J., 2006, Timing and prediction of CO₂ eruptions
731 from Crystal Geyser, UT: Lawrence Livermore National Laboratory. UCRL-TR, v. 221731, p.
732 16.
733
734 Gouveia, F.J., Johnson, M.R., Leif, R.N., and Friedmann, S.J., 2005, Aerometric
735 measurement and modeling of the mass of CO₂ emissions from Crystal Geyser,
736 Utah: Lawrence Livermore National Laboratory UCRL-TR, v. 211870, p. 59.
737
738 Grab, S. and Knight, J., 2015. Landscapes and landforms of South Africa – an overview. In:
739 Grab, S. and Knight, J. (eds), *Landscapes and landforms of South Africa*. World
740 Geomorphological Landscapes, Springer, Switzerland, 186pp.
741
742 Grunau, H. R. "A WORLDWIDE LOOK AT THE CAP-ROCK PROBLEM." *Journal of Petroleum*
743 *Geology* 10, no. 3 (1987): 245-265.
744
745 Haines, T.J., Michie, E.A.H., Neilson, J.E. & Healy, D. (2016). 'Permeability evolution across
746 carbonate hosted normal fault zones'. *Marine and Petroleum Geology*, vol 72, pp. 62-82.
747
748 Harris, C., Stock, W. D., & Lanham, J. 1997. Stable isotope constraints on the origin of CO₂
749 gas exhalations at Bongwan, Natal. *South African Journal of Geology*, 100(3), 261-266.
750
751 Hartnady, C. J. H. 1985. Uplift, faulting, seismicity, thermal spring and possible incipient
752 volcanic activity in the Lesotho-Natal Region, SE Africa: The Quathlamba Hotspot
753 Hypothesis. *Tectonics*, 4 (4), 371-377.
754
755 Healy, D., 2008. Damage patterns, stress rotations and pore fluid pressures in strike-slip
756 fault zones. *Journal of Geophysical Research: Solid Earth*, 113(B12).
757
758 Hesthammer, J., Johansen, T.E.S. and Watts, L., 2000. Spatial relationships within fault
759 damage zones in sandstone. *Marine and Petroleum Geology*, 17(8), pp.873-893.

760
 761 Hunter, A., & Donovan, S. 2005. Field sampling bias, museum collections and completeness
 762 of the fossil record. *Lethaia*, 38(4), 305-314.
 763
 764 Johnson, M.R., Anhaeusser, C.R. and Thomas, R.J. (Eds) 2006. The Geology of South Africa.
 765 Geological Society of South Africa, Johannesburg/Council for Geoscience, Pretoria, 691pp
 766
 767 Johnson, Kendra, Edwin Nissen, Srikanth Saripalli, J. Ramón Arrowsmith, Patrick McGarey,
 768 Katherine Scharer, Patrick Williams, and Kimberly Blisniuk. 2014. Rapid mapping of ultrafine
 769 fault zone topography with structure from motion." *Geosphere* 10, 969-986.
 770
 771 Kattenhorn, S.A., Aydin, A. and Pollard, D.D., 2000. Joints at high angles to normal fault
 772 strike: an explanation using 3-D numerical models of fault-perturbed stress fields. *Journal of*
 773 *Structural Geology*, 22(1), pp.1-23.
 774
 775 Kim, Y.S. and Sanderson, D.J., 2005. The relationship between displacement and length of
 776 faults: a review. *Earth-Science Reviews*, 68(3), pp.317-334.
 777
 778 King, L.C., 1972. The coastal plain of southern Africa: Its form, deposits and development:
 779 *Zeitschr. Geomorphologie*, N.F., Bd. 16, 239-251.
 780
 781 Kingsley, C.S. and Marshall., C.G.A., 2009. Lithostratigraphy of the Msikaba Formation (Cape
 782 Supergroup). South African Committee for Stratigraphy, Lithostratigraphic Series No. 50.
 783 Council for Geoscience, 8pp.
 784
 785 Krüger, M., Jones, D., Frerichs, J., Oppermann, B. I., West, J., Coombs, P., Green, K., Barlow,
 786 Y., Lister, R., Shaw, R., Strutt, M. and Möller, I. 2011. Effects of elevated CO₂ concentrations
 787 on the vegetation and microbial populations at a terrestrial CO₂ vent at Laacher See,
 788 Germany. *International Journal of Greenhouse Gas Control*, Vol. 5, 1093-1098.
 789
 790 Lake, L.W. (ed). 2007. Petroleum Engineering Handbook, Volumes I-VII. Society of Petroleum
 791 Engineers. Accessed via PetroWiki <http://petrowiki.org/PetroWiki>, May 2016.
 792
 793 Lawther, S.E., Dempster, T.J., Shipton, Z.K. and Boyce, A.J., 2016. Effective crustal
 794 permeability controls fault evolution: An integrated structural, mineralogical and isotopic
 795 study in granitic gneiss, Monte Rosa, northern Italy. *Tectonophysics*.
 796
 797 Li, S., M. Dong, Z. Li, S. Huang, H. Qing, and E. Nickel. 2005. Gas breakthrough pressure for
 798 hydrocarbon reservoir seal rocks: implications for the security of long-term CO₂ storage in
 799 the Weyburn field. *Geofluids* 5, 326-334.
 800
 801 Li, Z., Dong, M., Li, S., & Huang, S., 2006. CO₂ sequestration in depleted oil and gas
 802 reservoirs—caprock characterization and storage capacity. *Energy Conversion and*
 803 *Management*, 47(11), 1372-1382.
 804
 805 Manzocchi, T., Walsh, J.J., Nell, P. and Yielding, G., 1999. Fault transmissibility multipliers for
 806 flow simulation models. *Petroleum Geoscience*, 5(1), pp.53-63.

- McGrath, A.G. and Davison, I., 1995. Damage zone geometry around fault tips. *Journal of Structural Geology*, 17(7), pp.1011-1024.
- Metz, B., Davidson, O., De Coninck, H. C., Loos, M., & Meyer, L. A. (2005). IPCC, 2005: IPCC special report on carbon dioxide capture and storage. Prepared by Working Group III of the Intergovernmental Panel on Climate Change. *Cambridge, United Kingdom and New York, NY, USA*, 442.
- Miller, S.A., Collettini, C., Chiaraluce, L., Cocco, M., Barchi, M. and Kaus, B.J., 2004. Aftershocks driven by a high-pressure CO₂ source at depth. *Nature*, 427(6976), pp.724-727.
- Maud, R.R., 1961. A preliminary review of the structure of coastal Natal: Geological Society of South Africa. *Transactions of the Geological Society of South Africa*, 64, 247-256.
- Mauldon, M., Dunne, W.M. and Rohrbaugh, M.B., 2001. Circular scanlines and circular windows: new tools for characterizing the geometry of fracture traces. *Journal of Structural Geology*, 23(2), pp.247-258.
- Newell, D.L., Kaszuba, J.P., Viswanathan, H.S., Pawar, R.J. and Carpenter, T., 2008. Significance of carbonate buffers in natural waters reacting with supercritical CO₂: Implications for monitoring, measuring and verification (MMV) of geologic carbon sequestration. *Geophysical Research Letters*, 35(23).
- Otto, J.D.T., 1973. The geology and petrology of the Marble Delta. PhD thesis, University of Stellenbosch. 174pp.
- Partridge, T.C. and Maud, R.R. 2000. Macro-scale geomorphic evolution of southern Africa. In: T.C. Partridge and R.R. Maud (eds), *The Cenozoic of Southern Africa*. Oxford University Press, 3-18.
- Peacock, D.C.P., 2002. Propagation, interaction and linkage in normal fault systems. *Earth-Science Reviews*, 58(1), pp.121-142.
- Praetorius, B. and Schumacher, K., 2009. Greenhouse gas mitigation in a carbon constrained world: The role of carbon capture and storage. *Energy Policy*, 37(12), pp.5081-5093.
- Rinaldi, A.P. and Rutqvist, J., 2013. Modeling of deep fracture zone opening and transient ground surface uplift at KB-502 CO₂ injection well, In Salah, Algeria. *International Journal of Greenhouse Gas Control*, 12, pp.155-167.
- Ringrose, P.S., Mathieson, A.S., Wright, I.W., Selama, F., Hansen, O., Bissell, R., Saoula, N. and Midgley, J., 2013. The In Salah CO₂ storage project: lessons learned and knowledge transfer. *Energy Procedia*, 37, pp.6226-6236.

852 Roberts, J.J., Wood, R.A., Wilkinson, M. and Haszeldine, S., 2015. Surface controls on the
853 characteristics of natural CO₂ seeps: implications for engineered CO₂ stores. *Geofluids*,
854 15(3), pp.453-463.

855

856 Rohrbaugh Jr, M.B., Dunne, W.M. and Mauldon, M., 2002. Estimating fracture trace
857 intensity, density, and mean length using circular scan lines and windows. *AAPG bulletin*,
858 86(12), pp.2089-2104.

859

860 Roncella, R., Forlani, G., & Remondino, F. 2005. Photogrammetry for geological applications:
861 automatic retrieval of discontinuity orientation in rock slopes. In *Electronic Imaging*, p. 17-
862 27. International Society for Optics and Photonics.

863

864 Rotevatn, A. and Bastesen, E., 2014. Fault linkage and damage zone architecture in tight
865 carbonate rocks in the Suez Rift (Egypt): implications for permeability structure along
866 segmented normal faults. *Geological Society, London, Special Publications*, 374(1), pp.79-95.

867

868 Rutqvist, J., 2012. The geomechanics of CO₂ storage in deep sedimentary formations.
869 *Geotechnical and Geological Engineering*, 30(3), pp.525-551.

870

871 Salvini, Riccardo, Silvia Riccucci, Domenico Gulli, Riccardo Giovannini, Claudio Vanneschi,
872 and Mirko Francioni. 2015. "Geological application of UAV photogrammetry and terrestrial
873 laser scanning in marble quarrying (Apuan Alps, Italy)." In *Engineering Geology for Society
874 and Territory-Volume 5*, pp. 979-983. Springer International Publishing

875

876 Schlische, R.W., Young, S.S., Ackermann, R.V. and Gupta, A., 1996. Geometry and scaling
877 relations of a population of very small rift-related normal faults. *Geology*, 24(8), pp.683-686.

878

879 Shipton, Z.K. and Cowie, P.A., 2003. A conceptual model for the origin of fault damage zone
880 structures in high-porosity sandstone. *Journal of Structural Geology*, 25(3), pp.333-344.

881

882 Shipton, Z.K., Evans, J.P., Dockrill, B., Heath, J., Williams, A., Kirchner, D. and Kolesar, P.T.,
883 2006. Natural leaking CO₂-charged systems as analogs for failed geologic storage reservoirs.
884 *Carbon Dioxide Capture for Storage in Deep Geologic Formations-Results from the CO₂
885 Capture Project*, pp.699-712.

886

887 Shukla, R., Ranjith, P., Haque, A., & Choi, X. 2010. A review of studies on CO₂ sequestration
888 and caprock integrity. *Fuel*, 89(10), 2651-2664.

889

890 Sibson, R.H., 1995. Selective fault reactivation during basin inversion: potential for fluid
891 redistribution through fault-valve action. *Geological Society, London, Special Publications*,
892 88(1), pp.3-19.

893

894 Singh, V. and McLachlan, I. 2003. South Africa's east coast frontier offers untested mid- to
895 deepwater potential. *Oil and Gas Journal*, 101(22), 40-45.

896

897 Tamagawa, T. and Pollard, D.D., 2008. Fracture permeability created by perturbed stress
898 fields around active faults in a fractured basement reservoir. *AAPG bulletin*, 92(6), pp.743-

899 764.
900
901 Thomas, R.J., 1988. The geology of the Port Shepstone area. Explanation of sheet 3030
902 (1:250000). Geological Survey of South Africa, 136pp.
903
904 Thomas, R.J., von Brunn, V., Marshall, C.G.A., 1990. A tectono-sedimentary model for the
905 Dwyka Group in southern Natal, South Africa. *South African Journal of Geology*, 93, 809-
906
907 Verdon, J.P., Stork, A.L., Bissell, R.C., Bond, C.E. and Werner, M.J., 2015. Simulation of
908 seismic events induced by CO₂ injection at In Salah, Algeria. *Earth and Planetary Science*
909 *Letters*, 426, pp.118-129.
910
911 Von Veh, M.W. and Andersen, N.J.B., 1990. Normal-slip faulting in the coastal areas of
912 northern Natal and Zululand, South Africa. *South African Journal of Geology*, 93, 574-582.
913
914 Walker, R.J., Holdsworth, R.E., Imber, J., Faulkner, D.R., Armitage, P.J., 2013. Fault zone
915 architecture and fluid flow in interlayered basaltic volcanoclastic–crystalline sequences. *J.*
916 *Struct. Geol.* 51, 92–104.
917
918 Walsh, J. J. and Watterson J. 1988. Analysis of the relationship between displacements and
919 dimensions of faults. *J. Struct. Geol.*, 10, 239–247
920
921 Watkeys, M.K. and Sokoutis, D., 1998. Transtension in southeast Africa during Gondwana
922 break-up. In: Holdsworth, R.E., Strachan, R. and Dewey, J.F. (Eds), *Continental*
923 *Transpressional and Transtensional Tectonics*. Special Publication of the Geological Society
924 of London, 135, 203-214.
925
926 Watkins, H., Bond, C.E., Healy, D., Butler R.W.H., 2015. Appraisal of fracture sampling
927 methods and a new workflow to characterise heterogeneous fracture networks at outcrop.
928 *Journal of Structural Geology*, 72, 67-82.
929
930 Watts, N.L., 1987. Theoretical aspects of cap-rock and fault seals for single-and two-phase
931 hydrocarbon columns. *Marine and Petroleum Geology*, 4(4), pp.274-307.
932
933 Xu, T., Apps, J.A. and Pruess, K., 2003. Reactive geochemical transport simulation to study
934 mineral trapping for CO₂ disposal in deep arenaceous formations. *Journal of Geophysical*
935 *Research: Solid Earth*, 108(B2).
936
937 Yielding, G., Freeman, B. and Needham, D.T., 1997. Quantitative fault seal prediction. *AAPG*
938 *bulletin*, 81(6), pp.897-917.
939
940 Young R. B., 1924. Exhalations of Carbon Dioxide in Alfred County, Natal. *Transactions of the*
941 *Geological Society of South Africa*. 26, 99-102.
942
943 Ziogou, F., Gemeni, V., Koukoulas, N., de Angelis, D., Libertini, S., Beaubien, S.E., Lombardi,
944 S., West, J. M., Jones, D.G., Coombs, P., Barlow, T.S., Gwosdz, S. and Krüger, M. 2013.

Potential Environmental Impacts of CO₂ Leakage from the Study of Natural Analogue Sites in Europe. Energy Procedia, Vol. 37, 3521-3528.

Figure Captions

Figure 1. Location map of the field area and sites described. a) Outline of Africa, boxed area defines the location of map b. b) Outline of South Africa, grey box outlines map c. c) Geological map of the KwaZulu-Natal and Eastern Cape area of South Africa around Port Edward, after Gevers (1941), based on the mapping of du Toit (1920). d) Enlargement of the boxed area in c. showing the localities of the sites visited, and the local occurrence of CO₂ seeps.

Figure 2. Hypothetical models for permeability across fault zones. a) The fault core/slip-surface (red -line) is permeable and acts as a conduit for fluid. b) The fault core and the surrounding damage zone are permeable and act as a conduit for fluid. c) The fault core and/or slip surface is impermeable, but the surrounding damage zone is permeable and act as a conduit for fluid. d) permeability distribution is heterogeneous across the fault core and/or slip surface and the surrounding damage zone.

Figure 3. Structural data from the three field sites, shown in their spatial context with respect to the Bongwana Fault and CO₂ seeps. a) Geological map of the field area based on Gevers (1941) after the mapping of du Toit (1920), showing the spatial distribution of the three field sites, annotated with stereonet of measured fractures. b) Google Map satellite image showing the locations of images for Site B (figure part c) and Site C (figure part d), the fault trend mapped by du Toit and Gevers (1941) is shown by the white dashed line. Note the significant change in fault orientation between the sites. Stereonets show the mean fault-fracture orientation at Site Cii and Site Biv, and slickenside trend and plunge measurements (N=3 and N=14 respectively). c) Google Map satellite image of Site B, showing sub-sites i-iv and the associated fracture measurements at each sub-site. An approximate fault trend is shown by a dashed white line, star denotes site of CO₂ bubbles in the river. d) Google Map satellite image of Site C, showing sub-sites i-ii and the associated fracture measurements at each sub-site. Long dashed white line is the approximate fault trend, smaller dashed white lines outline travertine mounds around the Umtavuna River CO₂ exhalations. Present day CO₂ seeps are marked by white stars; the black star denotes the site of a now extinct CO₂ travertine cone. e) 3D photogrammetric image of the main active travertine cone, the cone is approximately 1.5m wide. All stereonet plots are equal area lower hemisphere projections (poles to fracture planes); rose plots, for the same fractures, are at 5 degree intervals.

Figure 4. Interpretations of fractures in orthorectified photographs created from virtual outcrop models. Each figure part shows the fracture interpretation and associated rose diagrams of fracture orientations, and a contour map of fracture density for each site. The sites are shown in figure 2 and are a) Site A, Fractures N=446; east fractures N=211, west fractures N=235; b) Site Bi, Fractures N=142; c) Site Biii, Fractures N=103; d) Site Ci, Fractures N=2285 and e) Site Cii, Fractures N=31.

Figure 5. Analysis of the effect of circle radius on fracture trace network parameters. a) Graph of fracture density, intensity and mean trace length against radius size. b) Location of circle centres used in the analysis on fracture trace map for site Ci.

Figure 6. The measured CO₂ ground flux at Site C. a) The aerial photograph shows the location of the nearby CO₂ seeps (white stars active travertine cones, black star non-active travertine cone). Coloured circles are measurement points scaled for gas flux and CO₂ concentration % in the soil. b) Actual measurements are shown in the inset graph.

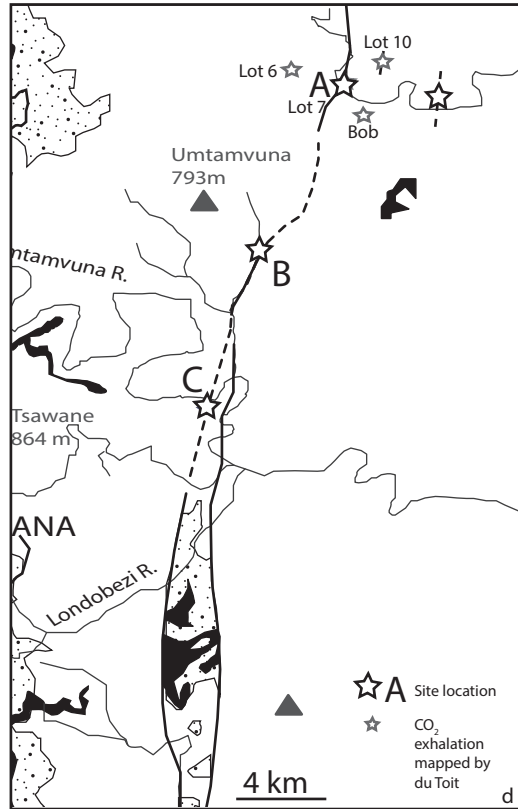
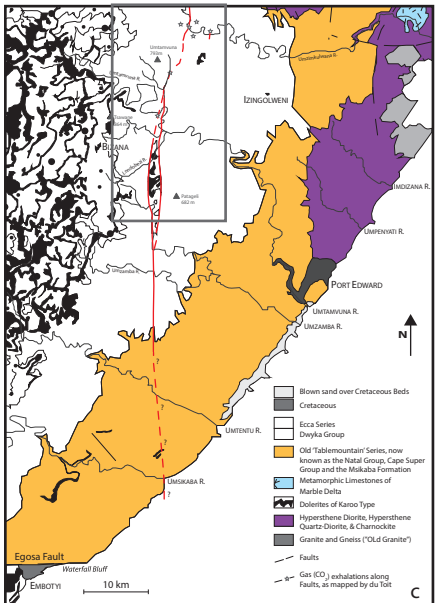
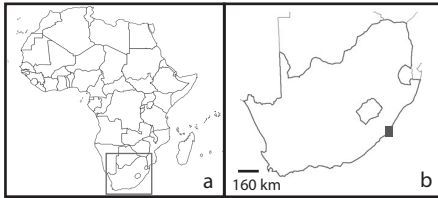
Figure 7. Porosity – log Permeability plot of sandstones. The plot shows the porosity-permeability ranges of sandstones from unconsolidated sands to tight sandstone, based on the Society of Petroleum Engineers, Petrowiki . The porosity and permeability values of the Msikaba Formation sandstone and Dwyka Group tillite are annotated.

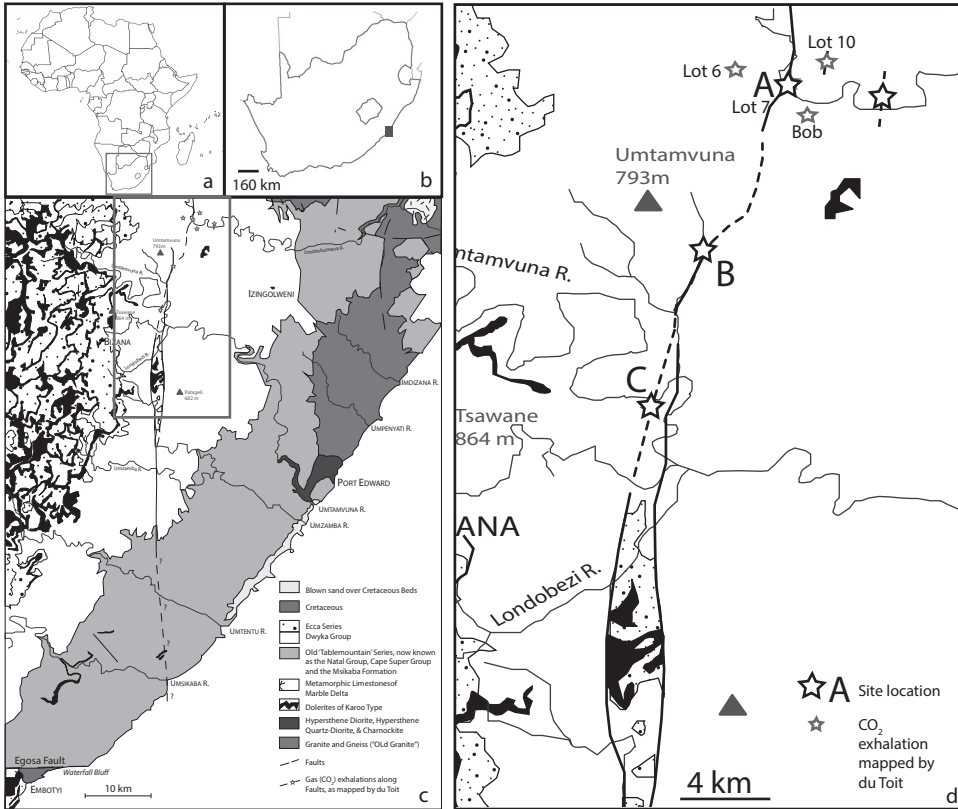
Figure 8. Summary model for CO₂ flow to the surface at the Bongwana Fault. a) Proposed model for a deep-seated fault connected to the surface via a fracture corridor. Complexities in fault geometry at depth, bends and asperities, create zones of more distributed damage observed in the fractures at the surface. This creates a more connected fracture network and a higher fracture permeability due to a greater range in fracture orientation. b) Simplified block model of a fault at depth (thin red line) with connection to the surface via a high permeability fracture network (black lines). The theoretical permeability graph, shows a potential range in permeability created by complexities in the fracture network that may control the leakage pathway for CO₂ to the surface.

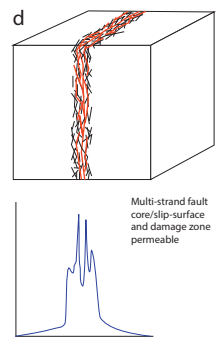
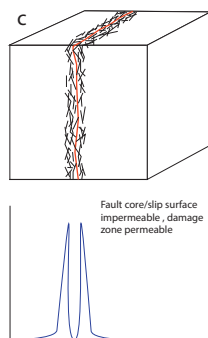
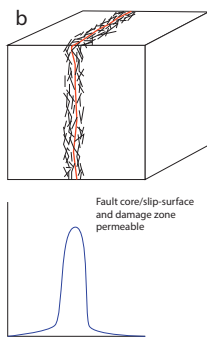
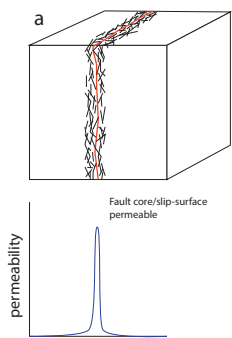
Table

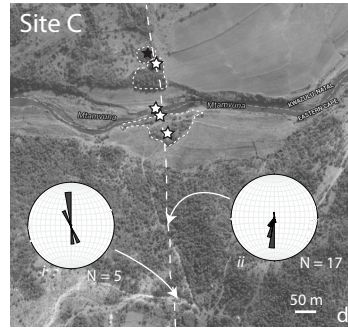
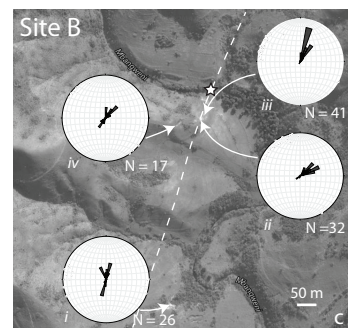
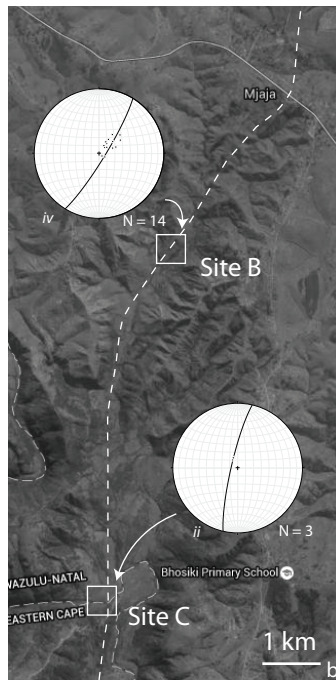
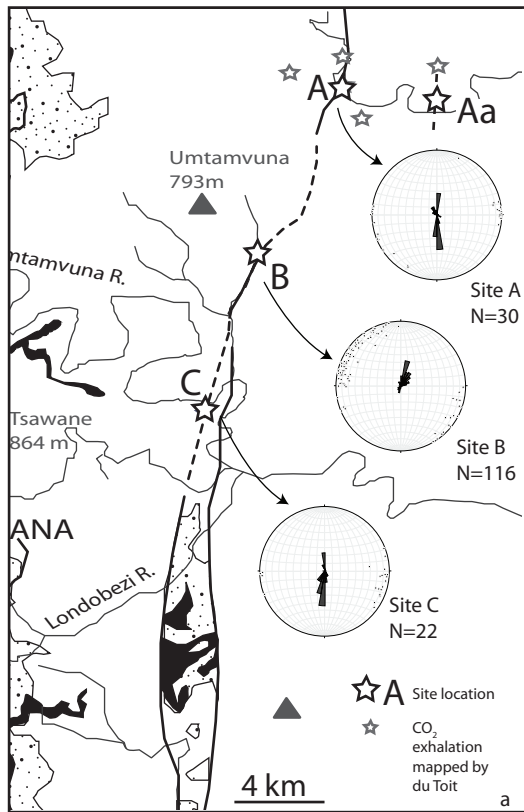
Sample	Porosity ϕ (He) %	Permeability – KL (N ₂)(mD)
<i>Msikaba Formation sandstone</i>		
20V –orthogonal to bedding	4.1	0.1865
20P – parallel to bedding	4.7	0.2762
20O – parallel to bedding orthogonal to 20P	4.4	0.2587
<i>Dwyka Group tillite</i>		
14V -vertical	22.8	0.0709
14O – orthogonal	21.2	0.0629

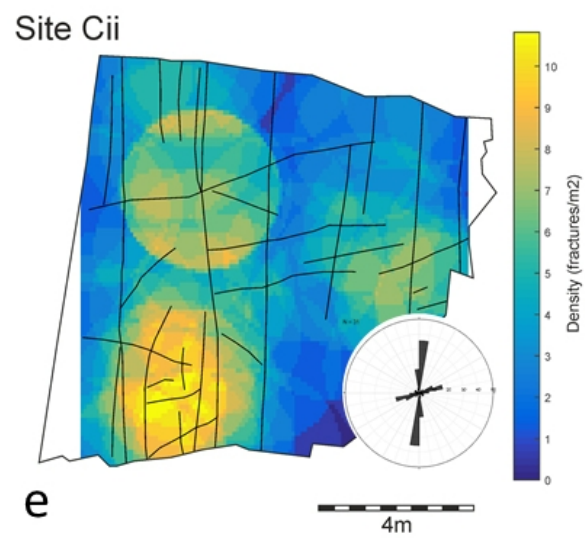
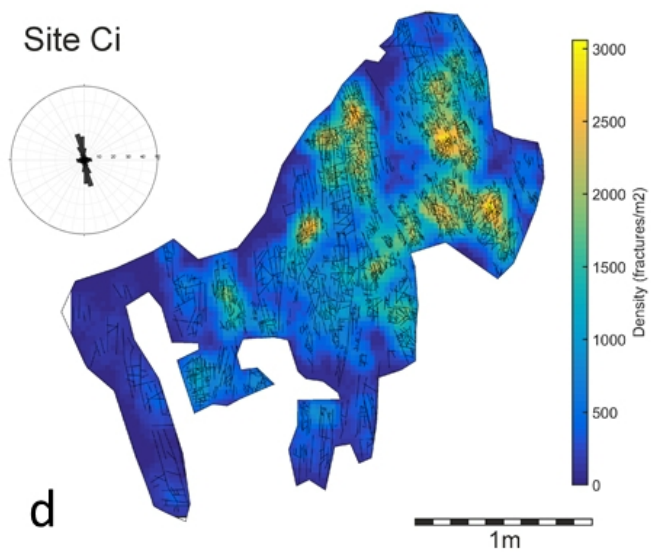
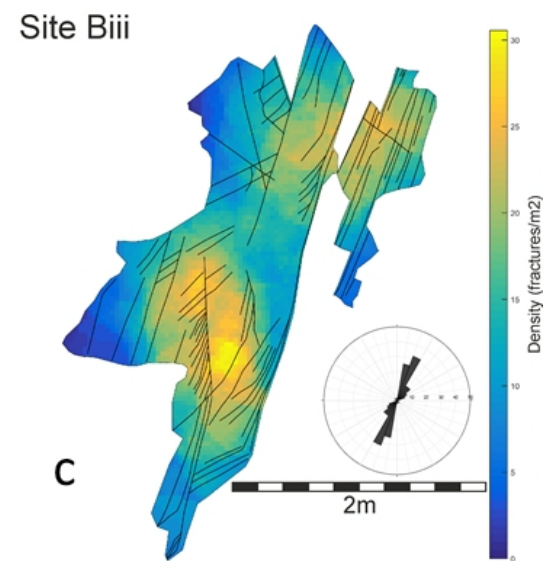
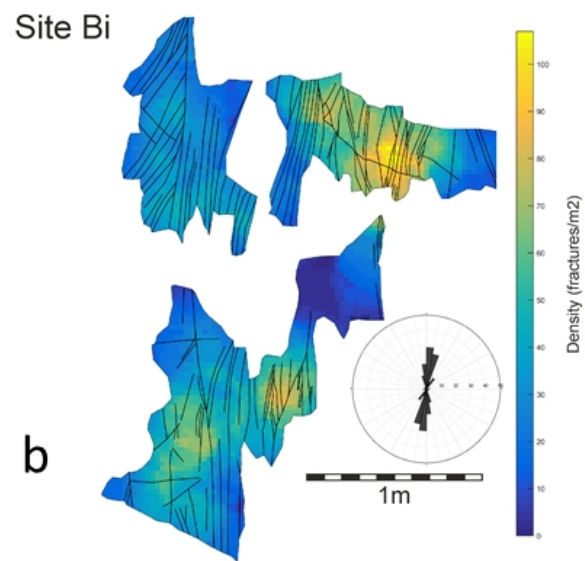
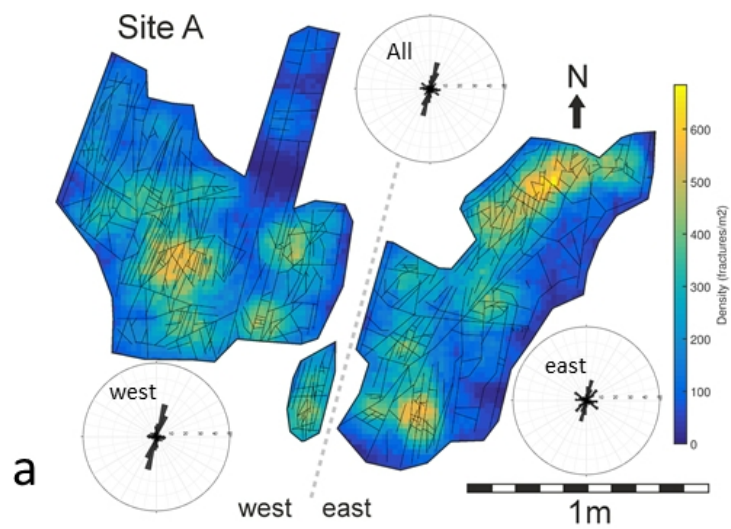
Table 1. Porosity and permeability measurements of the Msikaba Formation sandstone and Dwyka Group tillite.

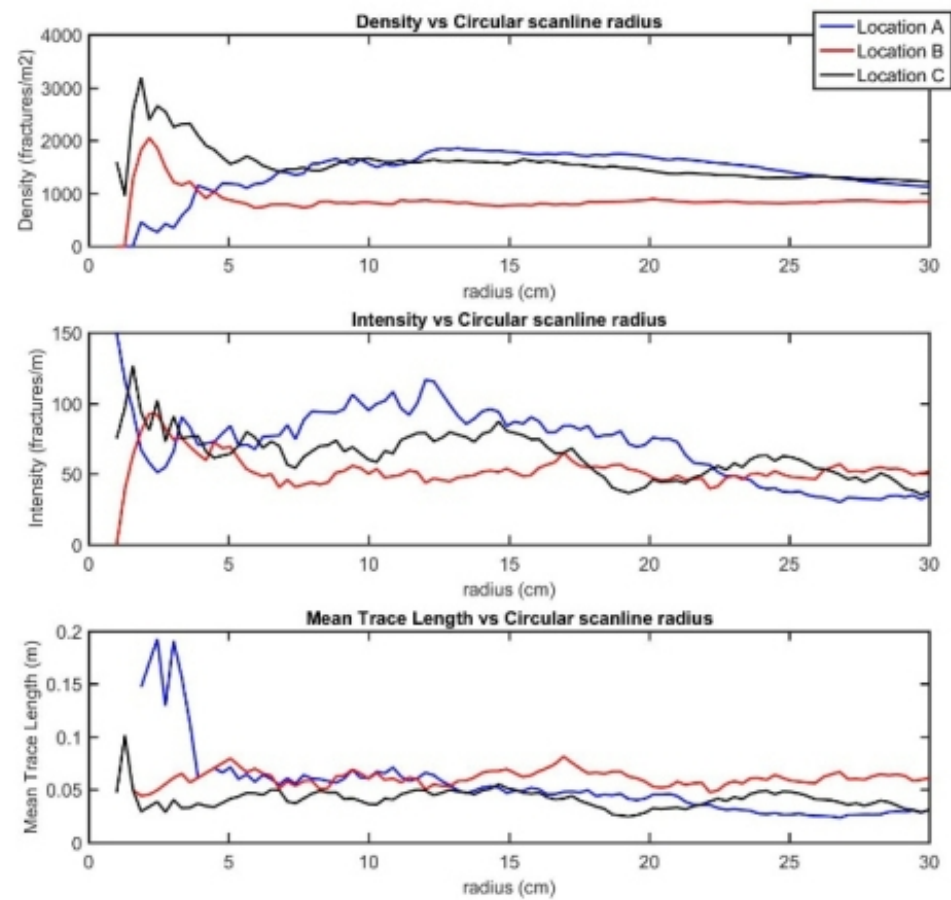




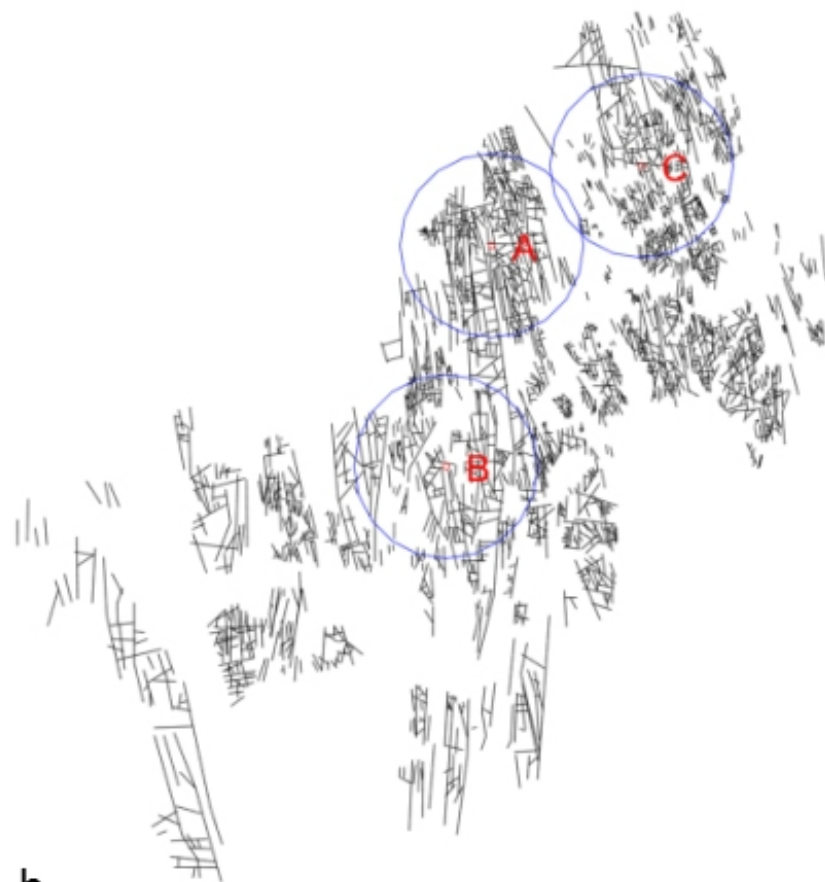






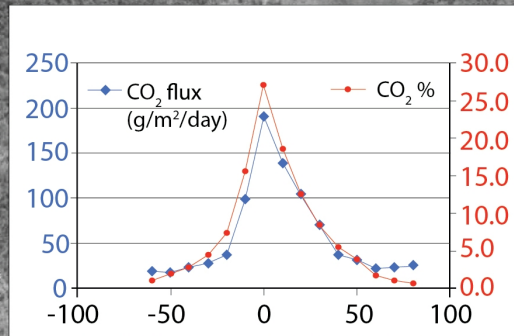
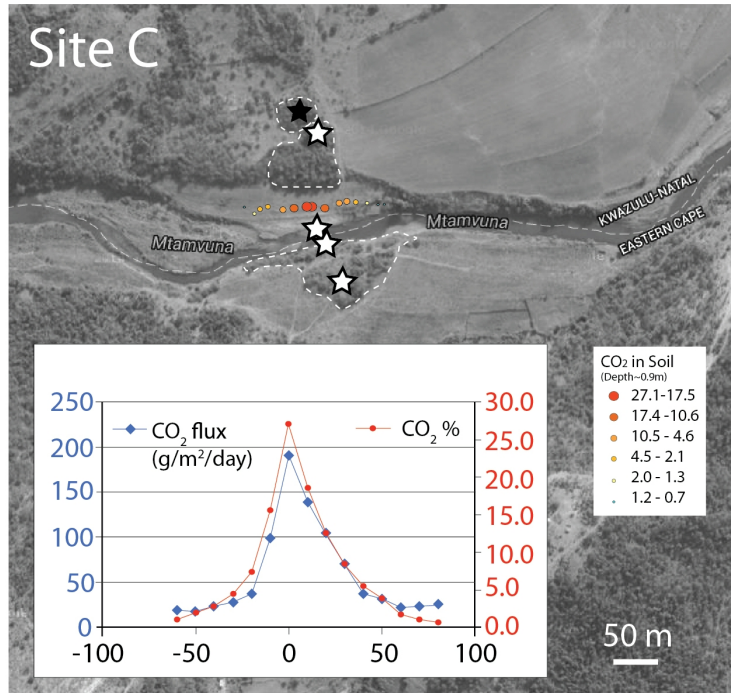


a



b

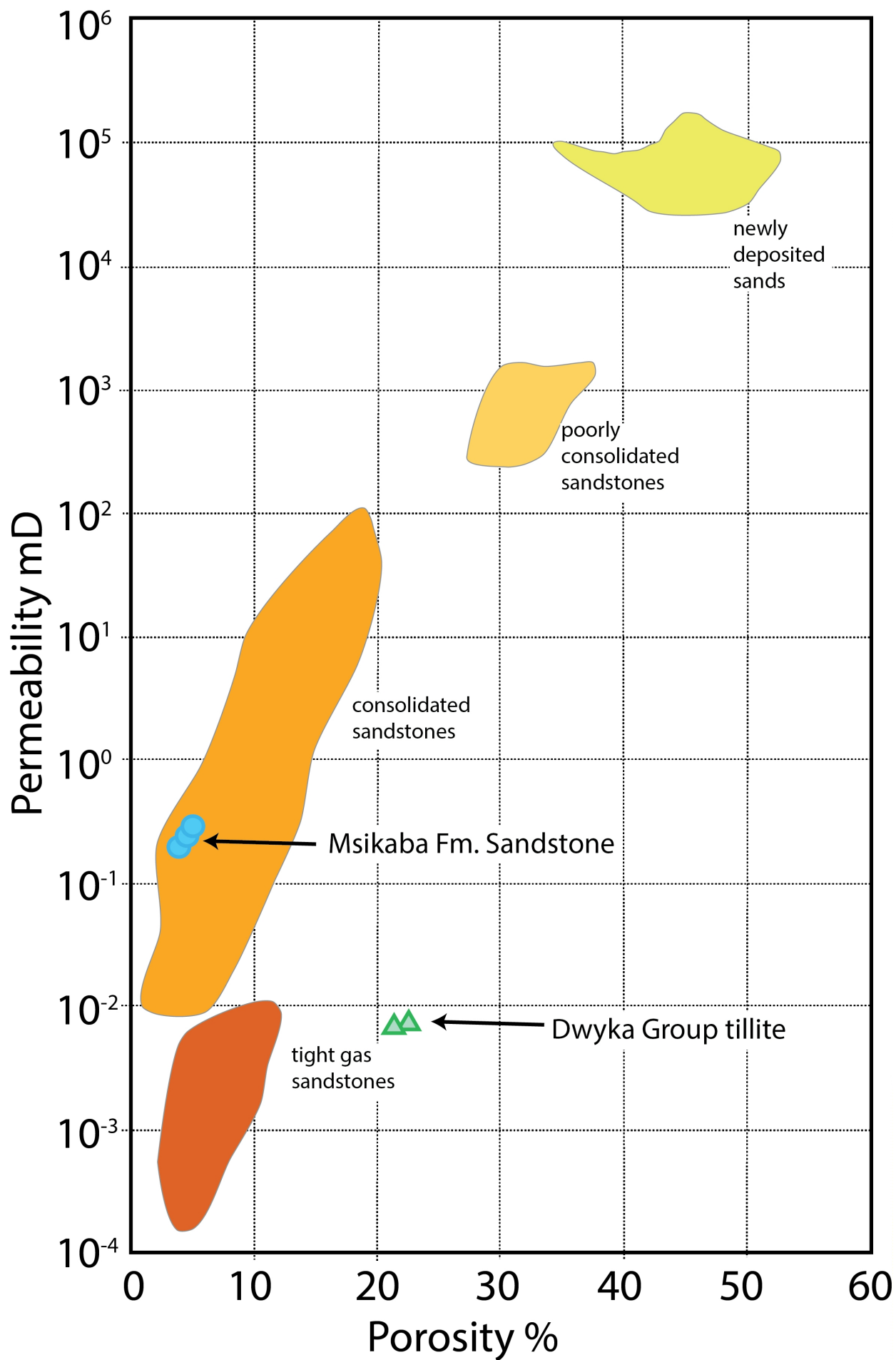
Site C



CO₂ in Soil
(Depth=0.9m)

- 27.1-17.5
- 17.4-10.6
- 10.5-4.6
- 4.5-2.1
- 2.0-1.3
- 1.2-0.7

50 m

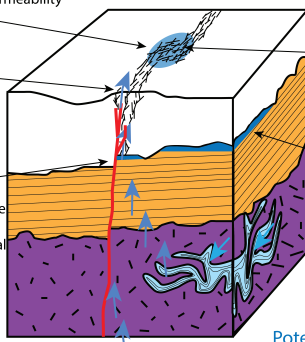


a

Multiple fracture orientations, and predicted high fracture permeability and CO₂ flux

CO₂ flow up fracture network to surface, in areas of fault complexity and splays

Juxtaposition of Dwyka Grp. tillite across the fault and high vertical fracture permeability minimises across fault CO₂ flow



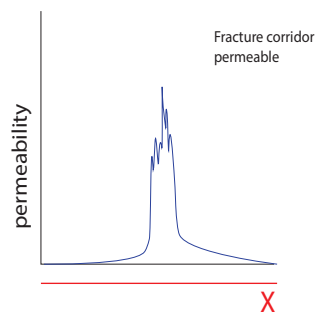
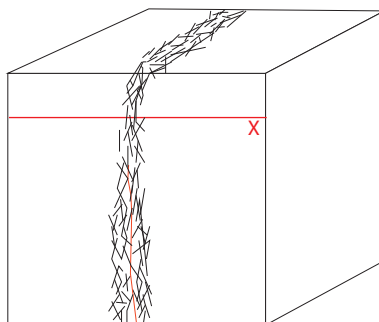
Bend in fault at depth - wider range in fracture orientation

CO₂ trapped in Msikaba Fm. Sst, unconformable base of Dwyka Grp. tillite provides a top seal away from the fault

H₂O reacts with marble - degasses CO₂

Potential CO₂ Sources

b



Highlights

- CO₂ migration is spatially associated with the Bongwana fault fracture corridor.
- Cap rock permeability suggests that without fractures it would act as a flow barrier.
- Elevated CO₂ concentration and flux are measured across the fracture corridor.
- Fracture intensity and orientation variability creates permeability heterogeneity.
- Seismically unresolvable fracture networks may impact CO₂ storage capability.